Airborne emission rate measurements validate remote sensing observations and emission inventories of western U.S. wildfires

Chelsea E. Stockwell[1,2], Megan M. Bela[1,2], Matthew M. Coggon [1,2], Georgios I. Gkatzelis [1,2,†], Elizabeth B. Wiggins[3], Emily M. Gargulinski[4], Taylor Shingler[3], Marta Fenn[3,5], Debora Griffin[6], Christopher D. Holmes[7], Xinxin Ye[8], Pablo E. Saide[8,9], Ilann Bourgeois[1,2], Jeff Peischl[1,2], Caroline C. Womack[1,2], Rebecca A. Washenfelder[2], Patrick R. Veres[2], J. Andrew Neuman[1,2], Jessica B. Gilman[2], Aaron Lamplugh[1,2], Rebecca H. Schwantes[1,2], Stuart A. McKeen[1,2], Armin Wisthaler[10,11], Felix Piel,[11,12], Hongyu Guo[1,13], Pedro Campuzano-Jost[1,13], Jose L. Jimenez[1,13], Alan Fried[14], Thomas F. Hanisco[15], L. Gregory Huey[16], Anne Perring[17], Joseph M. Katich[1,2], Glenn S. Diskin[3], John B. Nowak[3], T. Paul Bui[3], Hannah S. Halliday[18], Joshua P. DiGangi[3], Gabriel Pereira[19], Eric P. James[1,20], Ravan Ahmadov[1,20], Chris A. McLinden[6], Amber J. Soja[3,4], Richard H. Moore[3], Johnathan W. Hair[3], and Carsten Warneke[2]*

[1] Cooperative Institute for Research in Environmental Sciences, University of Colorado Boulder, Boulder, CO, USA

[2] NOAA Chemical Sciences Laboratory, Boulder, CO, USA

[3] NASA Langley Research Center, Hampton, VA, USA

[4] National Institute of Aerospace, Hampton, VA

[5] Science Systems and Applications, Inc., Hampton, VA, USA

[6] Air Quality Research Division, Environment and Climate Change Canada, Toronto, Ontario, Canada

[7] Department of Earth, Ocean, and Atmospheric Science, Florida State University, Tallahassee, FL, USA

[8] Department of Atmospheric and Oceanic Sciences, University of California, Los Angeles

[9] Institute of the Environment and Sustainability, University of California, Los Angeles
[10] Institute for Ion Physics and Applied Physics, University of Innsbruck, Innsbruck, Austria
[11] Department of Chemistry, University of Oslo, Oslo, Norway
[12] Ionicon Analytik, Innsbruck, Austria
[13] Department of Chemistry, University of Colorado Boulder, Boulder, CO, USA
[14] Institute of Arctic and Alpine Research (INSTAAR), University of Colorado Boulder, Boulder, CO, USA
[15] Atmospheric Chemistry and Dynamics Laboratory, NASA Goddard Space Flight Center, Greenbelt, MD, USA
[16] School of Earth and Atmospheric Science, Georgia Institute of Technology, Atlanta, Georgia, USA
[17] Department of Chemistry, Colgate University, Madison County, New York, USA
[18] Environmental Protection Agency, Research Triangle, NC, USA
[19] Department of Geosciences, Federal University of Sao Joao del-Rei, Sao Joao del-Rei, MG, Brazil
[20] NOAA Global Systems Laboratory, Boulder, CO, USA
[†] Now at Institute of Energy and Climate Research, IEK-8: Troposphere, Forschungszentrum Jülich GmbH, Jülich, Germany

*Email: Chelsea.Stockwell@noaa.gov; orcid.org/0000-0003-3462-2126

Keywords. Biomass burning, flux, total carbon, FIREX-AQ, remote sensing

Abstract. Carbonaceous emissions from wildfires are a dynamic mixture of gases and particles that have important impacts on air quality and climate. Emissions that feed atmospheric models are estimated using burned area and fire radiative power (FRP) methods that rely on satellite products. These approaches show wide variability, have large uncertainties, and their accuracy is challenging to evaluate due to limited aircraft and ground measurements. Here we present a novel method to estimate fire plume-integrated total carbon and speciated emission rates using a unique combination of lidar remote sensing aerosol extinction profiles and in situ measured carbon

constituents. We show strong agreement between these aircraft-derived emission rates of total carbon and a detailed burned area-based inventory that distributes carbon emissions in time using Geostationary Operational Environmental Satellite FRP observations (Fuel2Fire inventory, slope = 1.33 ± 0.04, r^2 = 0.93). Other commonly used inventories strongly correlate with aircraft-derived emissions, but have wide-ranging over- and under-predictions. A strong correlation is found between carbon monoxide emissions estimated in situ with those derived from the TROPOspheric Monitoring Instrument (TROPOMI) for five wildfires with coincident sampling windows (slope = 0.99 ± 0.18; bias = 28.5%). We report smoke emission coefficients (g MJ^{-1}) for many compounds including several previously unreported species. Smoke emission coefficients provide direct estimations of compound-specific emissions from satellite FRP observations.

Introduction

Biomass burning (BB) emits a complex mixture of carbon-containing gases and aerosols that play an important role in the global carbon cycle[1, 2]. As the frequency and severity of fire in the western U.S. continue to rise[3-6], accurate emission estimates of diverse constituents including aerosols, trace gases, and total carbon from fires are critical to evaluate the local, regional, and global impacts of BB on climate, weather, and air quality[7-9]. BB is the second largest global source of carbon dioxide (CO_2), total greenhouse gases, and trace gases, and is the largest source of primary carbonaceous particles to the atmosphere[10-13]. Carbon emissions released from BB are estimated to be ~20–40% of that released from fossil fuels[14, 15], although there is significant interannual variability and emission estimates vary by orders of magnitude with large uncertainties[16, 17].

Biomass burning emissions are commonly estimated using either “bottom-up” burned area or “top-down” FRP approaches. The conventional bottom-up methodology first outlined by Seiler and Crutzen[18] relies on biome-specific emission factors (EFs, grams emitted per kilogram of dry

fuel burned) for trace gases and aerosols and an estimate of the total amount of dry biomass consumed by the fire. The amount of biomass consumed is approximated from several parameters including burned area, fuel loading, and combustion completeness estimated from satellite products (hot spots, active fire counts, burn scars), derived from vegetation models[19], or predicted from environmental conditions (meteorology, fuel moisture) and/or fire processes (flaming/smoldering). Inventory estimates based on these methods often show large variability driven by uncertainties in fuel consumption estimates and inconsistencies in satellite products and fuel characteristics[19-24].

Top-down emission estimates rely on satellite fire radiative power (FRP) retrievals of a fire event. FRP-based approaches use the rate of energy released from fires as a proxy for emissions released from fuel consumption[25-29]. The total amount of dry biomass consumed by a fire can be estimated directly from the temporal integration of FRP (fire radiative energy, FRE; MJ) together with a scalar referred to as a biomass conversion factor (ß; kg dry mass burned MJ^{-1}) (Emissions [g] = β [kg MJ^{-1}] × FRE [MJ] × EF [g kg^{-1}]). β is derived experimentally from the linear relationship between directly measured fuel consumption and radiative energy released by a fire[26, 27, 30-33] or indirectly using satellite-FRP with model emission estimates or other emission products[34-36]. Alternatively, FRE can be directly translated to total emissions of individual constituents using compound-specific smoke emission coefficients[28, 37-40] (α; g MJ^{-1}) (Emissions [g] = α [g MJ^{-1}] × FRE [MJ]). FRP-based methods enable near-real time emission estimates, although because fires vary spatially, temporally, and in intensity, the spatiotemporal resolution of satellites adds uncertainty to FRP-derived products[41-43]. The emissions derived from both burned area (bottom-

97 up) and FRP-based (top-down) methods can differ by an order of magnitude and are challenging
98 to validate because of limited ground-based and in situ observations[22, 40, 41, 43, 44].

99 Emission rates (g s^{-1}) estimated from observations typically require knowledge of the entire
100 plume structure. Aircraft sampling of emission plumes generally only characterizes the horizontal
101 cross section of the plume, whereas the vertical distribution of species is typically unknown or
102 approximated. Airborne emission flux estimates computed using in situ measurements have only
103 been done within the planetary boundary layer (PBL), where emissions are assumed to be
104 uniformly mixed or the vertical structure of a plume is probed with multiple transects[45, 46]. In the
105 free troposphere, where many fire plumes are transported, it is challenging to estimate emission
106 fluxes using in situ measurements, since the vertical distribution of pollutants is typically
107 unmeasured. This study outlines a new approach to derive fire plume emission rates using the
108 combination of in situ measurements and lidar to resolve the horizontal and vertical distribution of
109 carbon in fire plumes.

110 This method is used to independently evaluate total carbon emissions derived from burned
111 area and FRP-based inventories, as well as carbon monoxide (CO) emission rates derived from the
112 TROPOspheric Monitor Instrument (TROPOMI) for western United States wildland fires. Nine
113 BB inventories are evaluated, including four burned area approaches, three traditional FRP-based
114 datasets, and two experimental products (in development) also based on FRP. Emission rates are
115 also derived for a variety of co-emitted compounds and are used to estimate smoke emission
116 coefficients using the relationship between total integrated emissions and integrated FRP for each
117 plume cross section. Emissions of several species are derived from aircraft measurements for the
118 first time and are expected to be representative of temperate forest ecosystems. The coefficients
119 can be applied in operational models that estimate primary emissions from satellite observations

of fire energy in order to predict ozone and secondary aerosol formation in temperate forest ecosystems or scaled for other ecosystems using appropriate emission factor ratios.

Materials and Methods

Campaign and measurement details. This study utilizes measurements collected aboard the NASA DC-8 aircraft during the western portion of the Fire Influence on Regional to Global Environments and Air Quality (FIREX-AQ) field campaign (Supporting Information (SI) Tables S1 and S2) that spanned thirteen flights sampling 10 distinct fires. This includes a suite of instrumentation quantifying gaseous and aerosol compounds, and a nadir/zenith directed Airborne Differential Absorption and High Spectral Resolution Lidar (DIAL-HSRL) to characterize the vertical distribution of aerosols and their optical properties (SI section S1.2). Total carbon is calculated as the sum of all background-subtracted carbon-containing gaseous and aerosol species measured in situ at one second time resolution (Eqn. S1). The three main carbon-containing emissions from fire (CO_2, CO, and CH_4) typically account for ~97–98% of the total carbon emitted[11, 47], and for the western U.S. wildfires sampled during FIREX-AQ, the average particulate contribution was less than 1%[48]. Additional information including fire selection, transect inclusion, and smoke age estimates is included in the SI.

In situ aircraft-derived emissions. Vertical total carbon concentration profiles are generated for each transverse plume crossing by scaling lidar spatial distributions of aerosol extinction (Mm^{-1}, 532 nm) to total carbon (ppbC) using an enhancement ratio of total carbon relative to in situ aerosol extinction at 532 nm measured aboard the aircraft. Missing data and gaps in the HSRL vertical extinction profiles resulted when plumes were too optically thick for the laser to fully penetrate, or when data were masked due to surface feedback or cloud coverage. Data gaps in the scaled carbon profiles are interpolated using a spatial interpolation method (Voronoi natural neighbor;

Figure S1). An example downwind flight track colored by in situ carbon is shown in Figure 1A together with the derived vertical carbon distributions (Figure 1B) shown for the same transect plume crossings.

The carbon emission rate (gC s^{-1}) is calculated for each HSRL pixel from carbon mass concentration (gC m^{-3}), pixel area (m^2), and horizontal wind speed (m s^{-1}) (Eqns. S2-S3). The total carbon emission rate (gC s^{-1}) through each plume cross section is estimated by summing vertically through the lidar sampling heights and horizontally across the width of the plume following Eqn. 1:

$$\text{Carbon Emission Rate (gC s}^{-1}) = \sum_{z=\text{surface}}^{z=20\text{km}} \sum_{t_{\text{entry}}}^{t_{\text{exit}}} \text{Conc. (gC m}^{-3}) \times \text{Area (m}^2) \times \text{Wind speed (m s}^{-1}) \quad (1)$$

where z is the altitude from the surface to 20 km above sea level and t is the aircraft sampling time from plume entry (t_{entry}) to exit (t_{exit}).

The error in scaling extinction to total carbon is estimated by comparing the scaled total carbon derived by HSRL measurements at the aircraft flight altitude with the sum of the onboard aircraft carbon measurements (average error across all fires ~38%). The error in scaling extinction to total carbon is propagated together with the uncertainty in the wind and results in a total measurement uncertainty that ranges by fire from 21 to 63%. Interpolating carbon concentrations through the plume center during lidar saturation likely results in some underestimation that may offset underestimation of onboard extinction measurements caused by evaporative inlet aerosol losses[49] that would bias scaled total carbon estimates high. A full description of these calculations, measurement descriptions, and uncertainties are provided in SI section S1.3.

The mass emission rates of individual species are determined as the product of the carbon emission rate and the transect-determined enhancement ratio of the individual constituent relative

to total carbon a. The total plume-integrated mass for nearly 90 compounds are derived from the compound-specific mass emission rate and total transect sampling time (Eqn. S5).

Biomass burning emission inventories. Nine biomass burning emission inventories are compared to the in situ observations of total carbon, including four burned area-based approaches: the campaign-specific high-resolution Fuel2Fire inventory (developed for this work and described further below), Global Fire Emissions Database (GFEDv4.1s)[24], the Brazilian Biomass Burning Emission Model updated to include emission factors from Andreae[50] (3BEM_A19), and the Fire INventory from NCAR (FINN v2.3)[51, 52]; three traditional FRP-based datasets: Global Fire Assimilation System (GFAS1.0)[35], Quick Fire Emissions Dataset (QFED2.4)[53], and Fire Energetics and Emissions Research (FEER)[37]; and also two experimental products (not fully operational at time of retrieval) based on FRP: High-Resolution Rapid Refresh (HRRR-Smoke v3)[54] and The Blended Global Biomass Burning Emissions Product (GBBEPx v3)[55]. Detailed information including spatial resolution, emission factor database references, and brief methodology descriptions are included in SI section S2.

The inventories provide daily biomass burning emissions summed for all inventory grid cells that at least partially overlap a circle with a radius of 0.25 degrees centered at the mean latitude and longitude of the United States Geospatial Multi-Agency Coordination (GeoMAC) fire perimeters hosted by the National Interagency Fire Center (https://data-nifc.opendata.arcgis.com/datasets/historic-perimeters-2019)[56]. Overlap is determined by identifying grid cells whose centers are within a radius of the GeoMAC fire perimeter mean latitude and longitude of 0.25 degrees plus one half of the diagonal length of the inventory grid cell (Eqns. S6 and S7).

TROPOspheric Monitoring Instrument (TROPOMI) CO emission estimates. TROPOMI orbits the western U.S. in a sun-synchronous orbit with equatorial crossing at 13:30 local time (LT) and retrieves total vertical column densities (VCDs) of CO. A cross-sectional flux method was applied to the CO VCDs to derive emission rates from single-orbit satellite observations, following the approach described by Adams et al.[57] and Griffin et al.[58]. Briefly, the VCDs are wind-rotated about the center of the fire location to obtain an upwind/downwind domain and binned into a grid (4 km × 4 km) that is background corrected using upwind CO observations. All grids within the fire plume boundary are integrated and an emission rate is estimated as the product of the mass enhancement and the wind speed. The total uncertainty of the CO emission estimates is approximately 40%. A detailed description of the TROPOMI CO emission method is included in SI section S3.2.

Results: Emissions validation and evaluation

Comparison of aircraft measurements with the FIREX-AQ Fuel2Fire inventory. The estimation of emission rates using the methods outlined above are only possible with a combination of remote sensing and in situ measurements on the aircraft. The derived carbon emission rates are compared to a comprehensive, burned area-based carbon emission inventory (Fuel2Fire). The Fuel2Fire inventory emissions are calculated using newly optimized methods specifically for the fires sampled during FIREX-AQ. Briefly, Fuel2Fire estimates the amount of fuel burned using active fire detections within a refined GeoMAC fire perimeter together with a high-resolution land classification system for fuel loading and fuel consumption determined from daily fire weather severity. By assuming a carbon fuel fraction, detailed daily carbon emission rates are estimated for each fire and are distributed temporally using FRP measured by the Geostationary Operational Environmental Satellite (GOES) (see SI section S3.1). Figure 2A shows

209 the 1 Hz Fuel2Fire carbon emission rates for the Williams Flats fire (August 3rd, 2019) along with
210 those based on airborne measurements (tonnes of carbon per second; tC s^{-1}). To align the aircraft
211 measurements to the Fuel2Fire emissions, the smoke age (SI section S1.5) is used to estimate the
212 original time of emission. The temporal variability prescribed to Fuel2Fire using geostationary
213 satellite FRP retrievals is captured well by the aircraft measurements for most transects. For other
214 fires, the magnitude of emissions is similar between methods, while individual data points show
215 large differences (Figure 2B), likely due to uncertainties in estimated smoke ages and uncertainties
216 in the GOES FRP retrievals (cloud/smoke obscuration, saturation, scan angle) used to distribute
217 emissions. Even with these outliers and emission rate uncertainties that range from 21 to 63% by
218 fire (SI section S1.3), the 15 min smoothed Fuel2Fire and aircraft measurements show agreement
219 using a reduced major axis regression (slope = 1.33 ± 0.04, r^2 = 0.92).
220 The described method captures plume heterogeneity and does not require the plume to be
221 mostly decoupled from the ground, which is necessary for airborne solar occultation flux
222 measurements[40, 59]. The use of lidar also reduces artifacts related to sampling plume cross sections
223 at altitudes that are not centered within the plume; however, the method assumes that all smoke
224 sampled in a vertical cross section was emitted simultaneously and transported/aged together,
225 which simplifies actual plume dynamics[60]. Even with these assumptions, the violin plots in Figure
226 2B and each fire time series in Figure S2 show this method and emission estimates using
227 Fuels2Fire agree in magnitude, show reasonable temporal variations in most sampled plumes, and
228 is appropriate for estimating emission rates from plumes that can be completely (or mostly)

penetrated by the lidar laser. In the following sections, these estimates are compared with satellite measurements of CO and then used to evaluate the accuracy of several BB emission inventories.

Comparison of aircraft measurements with TROPOMI satellite measurements. It is critical to validate satellite-derived BB emissions since satellite sensors have daily global coverage, and thus are essential for operational air quality and smoke models, whereas airborne and ground observations are infrequent and spatially limited. To date, TROPOMI CO retrievals have been validated by comparisons to ground-based, aircraft, and satellite remote-sensing measurements and model-simulated CO[61-65]. Previously, nitrogen oxides (NO_x)[58, 66] and nitrous acid (HONO)[67] biomass burning emissions have been derived from TROPOMI observations. This study is the first to evaluate TROPOMI-derived CO emissions from wildland fires by aircraft measurements. Here, fire-specific single-orbit TROPOMI CO emission estimates (SI section S3.2) near the fire source (within 20 km) are compared to the FIREX-AQ aircraft CO emission estimates. Aircraft-based plume-integrated CO emission rates are derived by scaling total carbon emission rates using the enhancement ratio of CO to total carbon for each transect (SI Eqn. S5). The aircraft-derived CO emission rates are averaged to include transects of the plume emitted within 90 minutes of the satellite orbit to have enough plumes to compare with and to account for uncertainties in the emission time. Figure 3 presents comparisons of TROPOMI CO emissions and aircraft-based estimates (tonnes of CO per hour, tCO h^{-1}) for the five fires measured during FIREX-AQ with coincident emission windows. The satellite shows agreement with the aircraft CO emission rate with a slope = 0.99. The average of the relative differences (bias=[TROPOMI-Aircraft]/Aircraft) was 28.5 ± 9.4 % (range ~2–59%), while the absolute differences range from 16 to 86 tCO h^{-1}. The horizontal bars show the temporal variability in the aircraft estimates within 90 min of the overpass that cannot be captured by the satellite, which shows that the aircraft measurements have

252 a finer spatial and temporal resolution than the satellite. The nitrogen oxide (NO) and nitrogen
253 dioxide (NO_2) fluxes estimated by this method were also used to evaluate TROPOMI NO_x
254 emission estimate methods as outlined by Griffin et al.[58]. Overall, the comparison of the
255 measurements with Fuel2Fire gives very high confidence in the accuracy of the total carbon
256 emission estimates from the DC-8 during FIREX-AQ and validates TROPOMI satellite-derived
257 CO emissions.
258 **Comparison with biomass burning emission inventories.** Conventional BB emissions
259 inventories use methods based on either burned area or satellite FRP and often incorporate other
260 satellite data products such as aerosol optical depth[25]. The magnitude and distribution of BB
261 emissions based on these methods vary widely and the availability of aircraft measurements to
262 evaluate inventory accuracy and uncertainty is very limited. To compare the aircraft measurements
263 with commonly used fire emission inventories, the daily total carbon inventory emissions are
264 distributed hourly using fire-day specific probability distributions estimated from GOES-FRP
265 diurnal patterns[68] (Figure S3) to isolate differences not related to inventory-applied fire diurnal
266 cycles. The GOES diurnals indicate limited nocturnal fire activity and therefore emission estimates
267 from all inventories are weighted towards the daytime. Total carbon emissions are calculated from
268 measurements for the Williams Flats fire on three separate days, and these aircraft measurements
269 are averaged to the hour to align with the inventories. The unweighted orthogonal distance
270 regressions between the aircraft- and satellite-based estimates are shown in Figure 4A. Nine BB
271 inventories including four burned area datasets (Fuel2Fire, GFED, 3BEM_A19, FINN), three
272 FRP-based inventories (GFAS, QFED, and FEER), and two experimental products also based on
273 FRP (HRRR-Smoke, GBBEPx)[22] are shown (SI section S2). The various inventories have a wide
274 range of emission estimates for the Williams Flats fire; for example, 3BEM_A19 is a factor of ten

lower and HRRR-Smoke a factor of three higher than the aircraft measurements, while the average of all inventory datasets lies near the one-to-one line (slope = 1.2). The Fuel2Fire and GFED inventory had the best overall agreement (slopes = 1.3 and 1.1, respectively), while the remaining FRP-based inventories had strong correlations, but are approximately a factor of 2 lower.

The magnitude of emissions on August 7th is 2–4 times larger than August 3rd, and the linear fits are driven by the higher emission day. The measurements and inventories for each plume crossing are averaged for each sampling day and Figure 4B shows the boxplot summaries (the median, 75th, and 25th quartiles or average ± standard deviation where n = 2). Emissions are the highest and most variable for the two experimental inventories, HRRR-Smoke and GBBEPx, while the remaining FRP-based inventories had better agreement and are within the 25th/75th quartile range of the aircraft measurements for both August 3rd and 7th, though below the average on the 7th. The emissions are lowest for all three of the burned area inventories on August 3rd (GFED, FINN, 3BEM_A19). On August 6th, all inventories are lower, while on the other days the inventory average agrees better with the measurements. Aircraft sampling on August 6th spanned only two hours (n=2) and the emission time was earlier than the highest FRP on that day, which may explain the low bias in all inventory emissions derived from the GOES diurnal emissions relative to aircraft measurements. This demonstrates that the prescribed fire diurnal cycle from GOES observations might not fully capture the fire diurnal cycle variability, especially during lower consumption periods. Many models use a fixed fire diurnal cycle for each day that can inaccurately distribute emissions[69] or weight emissions towards daytime hours[70], though these results show that even observationally-derived fire diurnal patterns can miss periods of emissions.

Every inventory except for the high-resolution Fuel2Fire inventory shows reduced daily emissions from August 7th to the pyrocumulonimbus event on August 8th (SI Figure S4, solid

298 lines). The primary difference between Fuel2Fire and the other inventories is that Fuel2Fire
299 assumes residual emissions from the area burned on the previous day; therefore, those days with
300 an intense preceding fire day will have higher relative emissions compared to other inventories.
301 Additionally, satellite products can severely underpredict emissions during large fire events due to
302 dense plumes concealing FRP or hotspots and need to consider fire behavior and changes in fuel
303 consumption.

304 Air quality forecast model predictions use the most recent satellite detections and typically
305 assume persistence into the forecasting window[69], and therefore most forecasts (Figure S4, dashed
306 lines) show increasing emissions from August 7th to August 8th. Forecasted total carbon emissions
307 for the Williams Flats fire, estimated from forecast carbon monoxide emissions with FIREX-AQ
308 derived CO emission factors, are compared to the inventory estimates in Figure S4. The forecasted
309 emissions vary by a factor of 35 and generally underpredict total carbon relative to the Fuel2Fire
310 inventory for most days, except for August 9th when Fuel2Fire indicates that the fire was subsiding
311 while forecasted persistence predict continued high emissions. Ye et al.[69] showed that
312 experimental models that ingested QFED emissions tend to have carbonaceous aerosol forecasted
313 emissions that are overpredicted relative to the Fuel2Fire inventory. One potential explanation for
314 these discrepancies is that Ye et al.[69] assumes a fixed percentage conversion from the Fuel2Fire
315 total carbon to carbonaceous aerosol that could bias the Fuel2Fire inventory low. Small
316 adjustments to this conversion factor can result in large differences in the predicted total aerosol
317 emissions. Additionally, the compound-specific emission factors used to estimate emissions vary

by model, and therefore the relative differences between forecasted emissions can vary by compound or conversion method.

The Williams Flats fire was the largest and most sampled fire during FIREX-AQ. The hourly comparisons for the other sampled western U.S. wildfires of various sizes are shown in Figure 5 with logarithmically-spaced histograms of the ratio of inventory to aircraft measurements. Only the FEER inventory missed estimates within the designated perimeter, and those data are included as zero emissions (n = 10). Inventory estimates are sensitive to the selected perimeter and defined overlap. For instance, GFED emission estimates, restricted to only include grid cells completely contained within a 0.25° radius circle of the fire location (no partial overlap), are zero across all sampled fires. The defined perimeter and overlap are described in SI section S2.1 and aim to capture each fire's total emissions without including any neighboring fires.

The Fuel2Fire and FINN inventories have more Gaussian distributions around the one-to-one ratio, while several traditional FRP-based inventories (GFAS, QFED, FEER) agree with geometric means ranging from 0.73 - 1.16, but have a larger spread in emissions (geometric standard deviation > 3.5). Generally, the GFED inventory underpredicts emissions (0.45 ± 3.60), but has less fire-to-fire variability than the 3BEM_A19 burned area inventory (0.19 ± 9.71), whose spread in emissions were driven by overpredictions during the Tucker and North Hills fires. The latest version of GFED uses the Moderate Resolution Imaging Spectroradiometer (MODIS) burned area product together with additional algorithms in order to capture small fires, however, there are large uncertainties even with improvements[71, 72]. The recent version of FINN (v2.3) applies updated burned area estimates from MODIS plus the Visible Infrared Imaging Radiometer Suite (VIIRS) fire detects and generally has higher emissions than its predecessor for temperate North America[52], though it continues to underpredict emissions relative to the aircraft (0.65 ±

341 3.45). These advances in burned area estimates reduce some of the low bias frequently observed
342 for these inventory types in some regions[22]. In general, these three burned area inventories more
343 frequently underpredict emissions relative to the aircraft, yet can agree well on a per-fire basis
344 (e.g., the Williams Flats fire). HRRR-Smoke and GBBEPx have the highest overall emissions and
345 significant variability. As an example, GBBEPx agrees well for the Williams Flats fire (Figure
346 4A), but overpredicts relative to aircraft-derived total carbon by a factor of 4 for the Sheridan fire.
347 A potential reason for the difference could be the inventory-assigned (QFED) land-cover
348 classification, since the Sheridan fire on August 16th is categorized as a mix of savanna and
349 extratropical forest, while the Williams Flats fire is exclusively extratropical forest.

350 Estimated values of the energy released from burning fuel (biomass conversion factor, β)
351 are used in several FRP-based approaches to estimate the amount of dry mass burned, although β
352 values vary by detection method and have been scaled to match burned area generated emissions
353 for several fuel types[35]. GFAS, QFED, and FEER had similar distributions in emissions, and
354 agreement with field observations would potentially improve with updated biomass
355 conversion/smoke emission coefficients or by implementing higher temporal and spatial resolution
356 satellite FRP retrievals (e.g., GOES or hybrid/fused FRP products).

357 **Results: Speciated emissions**

358 **Smoke emission coefficients.** FRP-based emission estimates for all compounds in smoke rely on
359 either a biomass conversion factor (β; kg dry mass burned MJ^{-1}) together with biome-specific
360 emission factors (EFs) or compound-specific (X) smoke emission coefficients (α, gX MJ^{-1}). Smoke

emission coefficients are empirically derived from laboratory measurements[28], satellite retrievals[38, 42, 73], and/or chemical transport models[74].

Each measured carbon species is integrated over the time needed to complete an individual plume transect to obtain a total mass for each transect. Emission coefficients (α-values) are then calculated from the total mass for each transect against the transect-specific FRE (time-integrated FRP) as shown in Figure 6A for total carbon and Figure 6B for CO. The smoke emission coefficients for total carbon ($\alpha = 105.9 \pm 10.9$ g MJ^{-1}), CO ($\alpha = 21.4 \pm 2.2$ g MJ^{-1}), and many other previously-unmeasured compounds are listed in SI Table S3 for temperate forest fuels. Secondary products that are not expected to be primarily emitted are excluded (e.g., ozone, peroxyacylnitrates, HNO_3). These are the first reported emission coefficients using in situ aircraft measurements for large-scale wildfires. Additional details including descriptions of excluded fires and transects are detailed in SI section S1.6.

Figure 6B also shows the TROPOMI-derived total CO mass (red) versus GOES-integrated FRP has a similar CO α-value (23.9 ± 7.0 g MJ^{-1}) as those derived using aircraft measurements (21.4 g MJ^{-1}). The TROPOMI value is comparable to the value derived for the continental United States (CONUS) using TROPOMI CO total mass with GOES FRP from 41 fires (29.92 g MJ^{-1})[42] and a laboratory-derived value (33.71 g MJ^{-1})[28], further validating the aircraft method. Previous CO emission coefficients calculated using satellite particulate matter emission coefficients scaled to CO using emissions factors are much higher (105–192 g MJ^{-1}) and lead to higher emission estimates[25, 37, 75].

Figure 6B also shows the TROPOMI CO estimates versus FRP from MODIS Aqua retrievals for western U.S. fires sampled during FIREX-AQ and another western U.S. wildfire campaign (WE-CAN; Western Wildfires Experiment for Cloud Chemistry, Aerosol Absorption,

and Nitrogen[76]; SI S3.2) assuming a 40% uncertainty in both (blue, α value = 31.5 ± 6.7 g CO MJ^{-1}, $r^2 = 0.72$). The overpass times of the two satellites are not always coincident, though their orbits are generally within 2 h. The relative difference between the satellite FRP-products (MODIS vs. GOES) was only ~21%. Using the CO α-value to predict WE-CAN emissions shows agreement with TROPOMI (~55% difference on average), and therefore using these α-values in GOES or MODIS FRP-based operational models is representative for temperate forest ecosystems, although differences for individual fires will exist. The methods outlined in this study could be used to derive α-values for other ecosystems. Alternatively, the temperate forest values could be scaled by multiplying by the ratio of ecosystem-specific emission factors for each selected constituent (X) taken from biomass burning emission databases (i.e., $EF_{X,\ ecosystem}$ /$EF_{X,\ temperate\ ecosystem}$)[11, 50].

With the method described here, the biomass conversion factor, which represents the amount of fuel burned per energy released, cannot be measured directly since the amount of fuel consumed is unmeasured. The factor was instead calculated as the average of the ratios of smoke emission coefficients to the campaign-wide average EFs for all species measured by the DC-8 as reported by Gkatzelis et al.[48]. The resulting biomass conversion factor was 0.21 ± 0.10 kg MJ^{-1}, which is lower than laboratory/controlled fires (0.368–0.453 kg MJ^{-1})[26, 28, 77] or satellite/model emission derived values for extratropical forest/temperate fuels (0.261–0.49 kg MJ^{-1})[32, 35]. β-values vary widely among satellite-based studies by vegetation-type or by FRP-product (0.13–12 kg MJ^{-1})[26, 28, 32, 36, 38, 41, 43, 77-79], which again highlights the need for aircraft measurements such as those flown during FIREX-AQ for other ecosystems.

The FRP / total reactive nitrogen oxides (NO_y) relationship. The outlined methods have focused on carbon emissions, though quantifying both carbon-containing volatile organic compounds (VOCs) and nitrogen oxides (NO_x) and other reactive nitrogen species is critical for

understanding the air quality and climate impacts of ozone and secondary organic aerosol (SOA) formation downwind of wildfires[80]. Total reactive nitrogen oxides (NO_y) is a reasonably-conserved tracer in smoke plumes[81] and the ratio of VOCs to NO_y can be used as a proxy for downwind ozone formation from wildfires as the initial mix of emissions controls NO_x loss pathways, which will determine the chemical regimes (NO_x-sensitive or VOC-sensitive) of the downwind plume[80]. Gkatzelis et al.[48] demonstrate that VOCs from fresh plumes can be estimated using direct CO measurements near the fire source while the NO_y relationship with CO is less correlated across all fires sampled ($r^2 = 0.75$) . Figure 6C shows that total transect integrated NO_y (g) has a strong relationship with integrated FRP ($r^2 = 0.91$) for the temperate fuels, and because NO_y is conserved in the absence of wet or dry deposition, the correlations hold for both fresh and aged plumes (colored by smoke age). The initial concentrations of VOCs can then be estimated from parameterizations of satellite-measured CO (TROPOMI or Cross-track Infrared Sounder [CrIS]), while total NO_y can be estimated from integrated FRP satellite retrievals (MODIS/GOES/VIIRS) using the predicted emission coefficient for the temperate ecosystem. More work is needed to investigate differences between ecosystems and/or burn conditions (i.e., fuel moisture, meteorology), though there were no apparent trends with modified combustion efficiency identified here. Predicting and implementing the initial concentrations of VOCs and NO_y from satellite products (CO and FRP) into models might enable more accurate and simplified estimates of downwind ozone and SOA formation without the need for direct field measurements.

Discussion

The wide variability and large uncertainty in biomass burning emission estimates by inventories complicate the interpretation of fire impacts on air quality and climate. Evaluating the accuracy of commonly used biomass burning emission inventories has traditionally been challenging due to

limited in situ aircraft or ground-based measurements. This study presents a new method of calculating emission rates using in situ and remote-sensing airborne measurements, which were compared to various inventories. The high-resolution burned area-based estimates generated for FIREX-AQ (Fuel2Fire) accurately predict western wildland fire emissions, yet are very time intensive to generate. Emissions from other traditional inventories vary greatly, resulting in both over- and under-predictions of emissions when compared to the aircraft-derived method. We derive in situ smoke emission coefficients from wildfire plumes using lidar to determine the plume's spatial extent. The aircraft-derived smoke emission coefficients can replace emission factors to estimate fire emissions directly from satellite FRP, bypassing fuel burned estimates. The outlined method can be used to derive coefficients for other ecosystems directly or the presented values can be scaled using the appropriate ratio of EFs. In situ aircraft measurement derived emission coefficients are reported for the first time for a wide range of species and implementing these values in air quality and smoke models is expected to improve the accuracy and spatial coverage as inventories begin to utilize higher time resolution geostationary FRP retrievals.

Figures and Tables

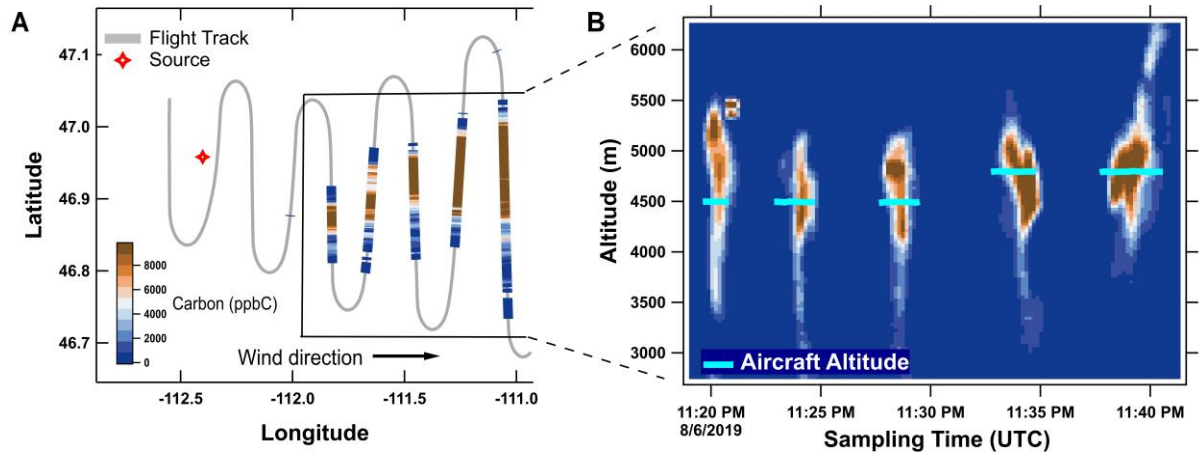

Figure 1. (A) The DC-8 flight track showing several transverse transects of the Horsefly fire plume (August 6, 2019) colored by the sum of in situ aircraft measurements of excess carbon (ppbC). (B) An example vertical profile of transect plume crossings colored using the same color scale shown in panel A. The aircraft sampling altitude above mean sea level (m) is indicated by the cyan line.

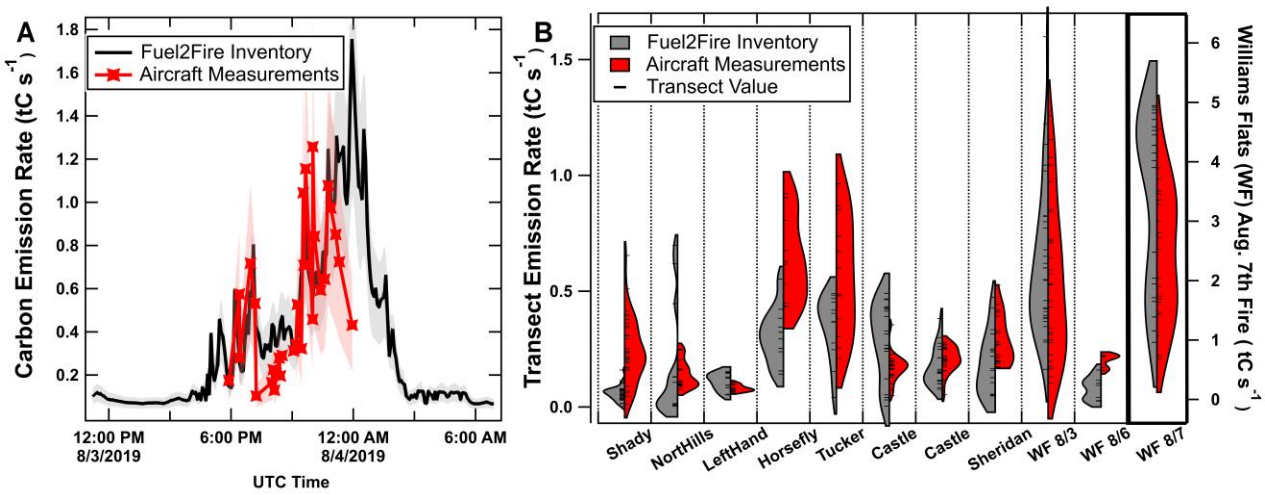

Figure 2. (A) Total carbon emission rates determined for the DC-8 aircraft transects (red) and the Fuel2Fire daily carbon burned area estimate partitioned onto a 1s time base (black) using the GOES-derived FRP diurnal pattern for the Williams Flats fire on August 3rd, 2019. (B) Violin plots showing the distribution of individual transect emission rates (black lines) taken from 15 min smoothed Fuel2Fire carbon estimates (grey) and aircraft measurements (red) at the estimated time of emission using a Gaussian kernel.

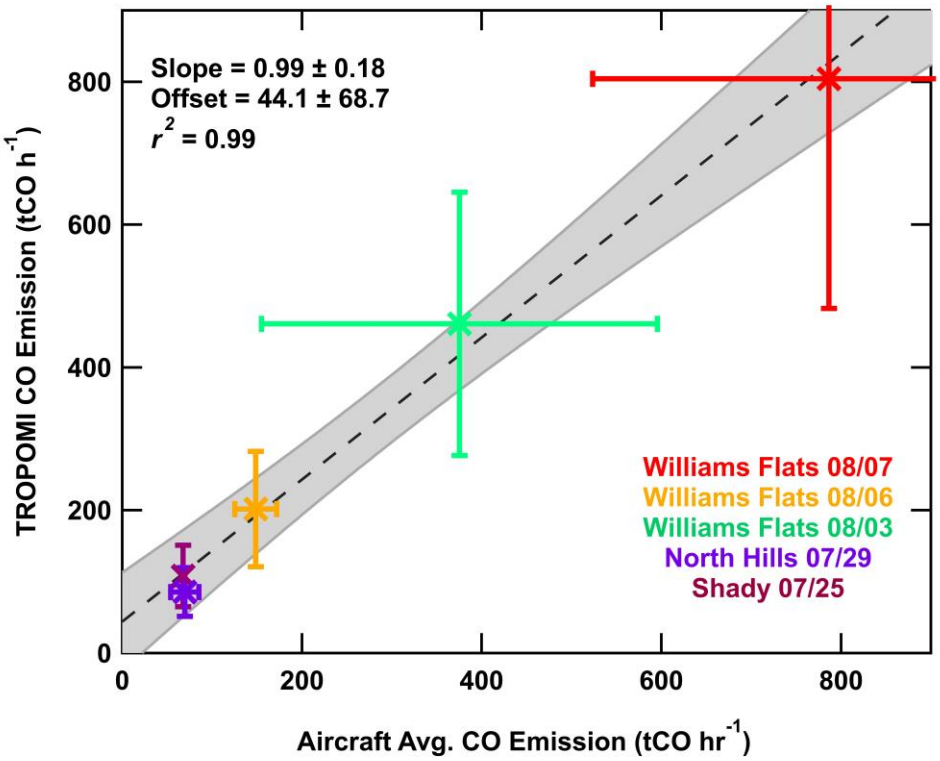

458
459 **Figure 3.** Correlation between TROPOMI CO and aircraft CO emission rate estimates (tCO h^{-1})
460 averaged when smoke emission times were within 90 minutes of the satellite overpass (~13:30
461 LT) for the North Hills (n=2), Shady (n=1), and Williams Flats fires on August 3rd (n=10), 6th
462 (n=5), and 7th (n=5). The 95th confidence intervals in the slope (grey), ± standard error of aircraft
463 data (horizontal bars), and a 40% error in the TROPOMI CO estimate[58] (vertical bars) are shown.
464

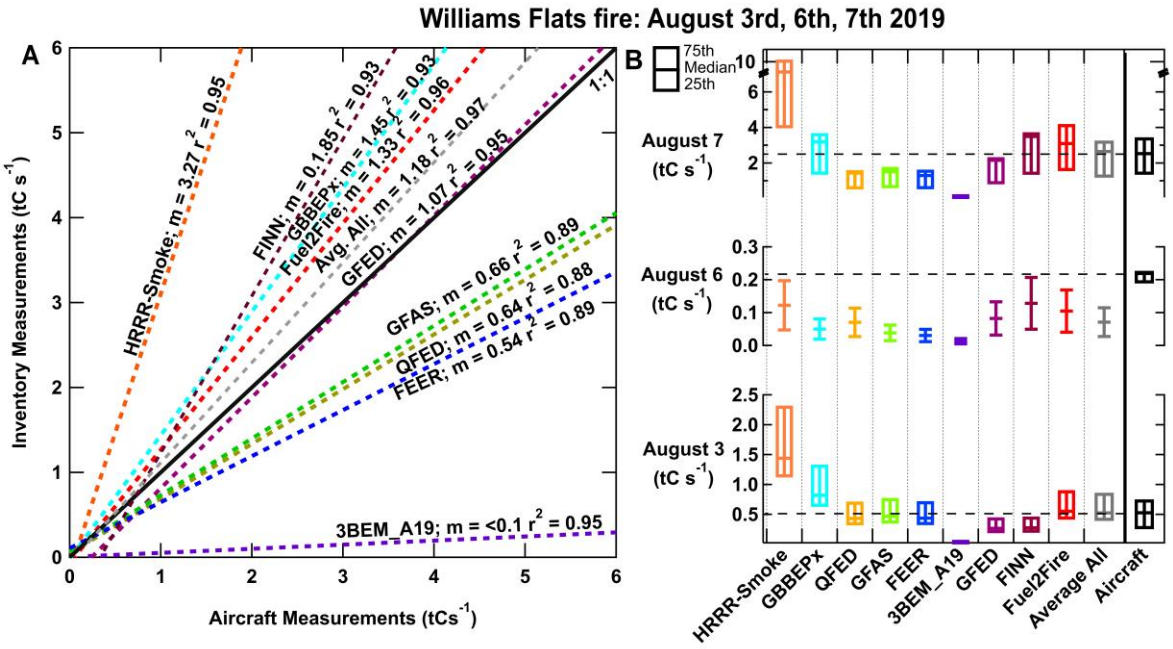

Figure 4. (A) Orthogonal distance regression fits of inventory emissions against aircraft measurements averaged to the hour for three flights sampling the Williams Flats fire. (B) All aircraft measurements (black) and inventory emissions (colored) were binned during the aircraft sampling period (2–7 h) for the Williams Flats fire. The median, 75th, and 25th quartiles are shown, or the average ± 1 standard deviation where n = 2 (August 6th).

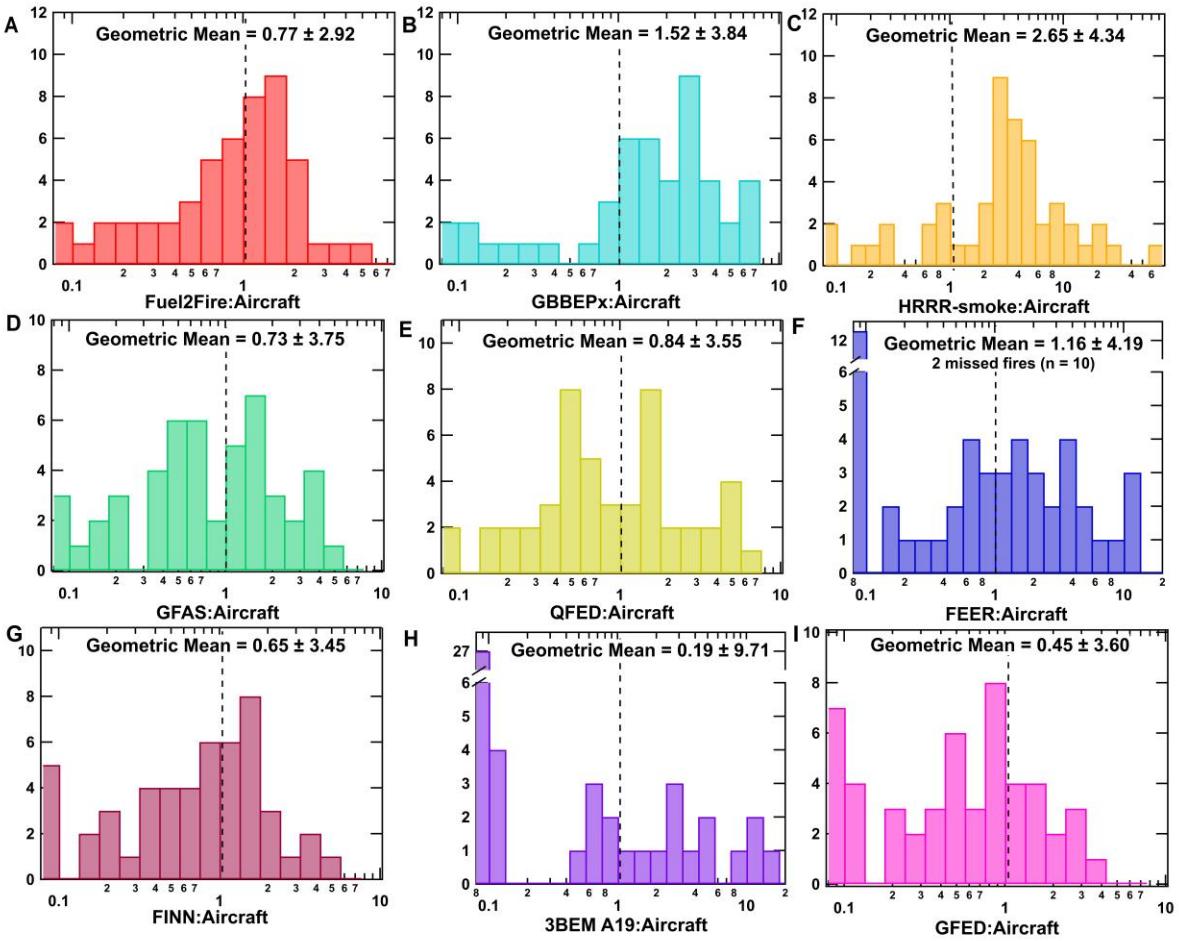

Figure 5. Distribution of the ratio of inventory carbon emissions to aircraft carbon measurements for hourly-averaged observations of 11 fires for Fuel2Fire (red), GBBEPx (cyan), HRRR-Smoke (orange), GFAS (green), QFED (yellow), FEER (blue), FINN (maroon), 3BEM_A19 (purple), and GFED (pink). The one-to-one ratio is shown as a dashed line. The geometric mean ± geometric standard deviation is listed for each inventory.

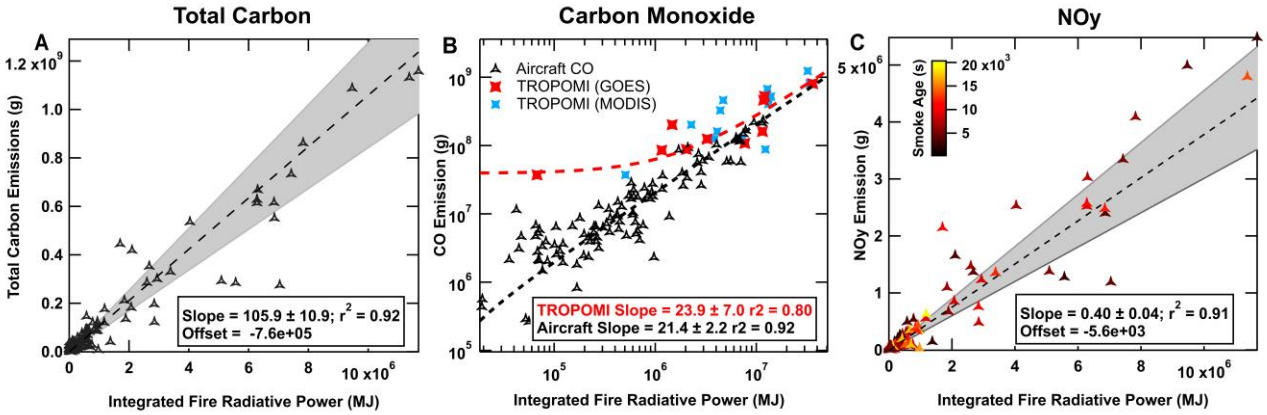

Figure 6. (A) Total carbon emissions (g) versus integrated fire radiative power (MJ) used to generate a smoke emission coefficient for carbon (gC MJ^{-1}) from a York regression fit (dashed line) with the 95% confidence intervals shown (shaded grey). (B) CO emission (g) versus GOES integrated FRP for aircraft measurements (black) and TROPOMI retrievals (red). Emissions versus MODIS-Aqua integrated FRP for TROPOMI, FIREX-AQ, and WE-CAN fires are shown where available (blue) (C) NO_y emission versus integrated FRP colored by smoke age.

Supporting Information. Extended experimental methods, biomass burning emissions inventory descriptions, satellite retrieval descriptions, and a summary of forecast models is included in the Supporting Information (SI) and Tables S1-S4 and Figures S1-S4.

Corresponding Author. Chelsea E. Stockwell; Cooperative Institute for Research in Environmental Sciences, University of Colorado, Boulder, CO, United States; NOAA Chemical Sciences Laboratory, Boulder, CO, United States; orcid.org/0000-0003-3462-2126

Author Contributions. CW organized field measurements and supervised the research; MMC and GIG conducted PTR-ToF-MS measurements; MMB calculated daily inventory estimates; CDH estimated smoke ages; IB and JP conducted NOyO3 measurements; CCW and RAW performed ACES measurements; PRV and JAN conducted I-CIMS measurements; JBG and AL conducted GC-MS measurements; AW and FP conducted additional PTR-MS measurements; JLJ, PCJ and HG conducted AMS measurements; AF conducted CAMS measurements; TFH conducted ISAF measurements; LGH conducted I-CIMS measurements; GSD, HSH, JBN, and JPD conducted CO, CO2, and CH4 measurements using a LICOR and DACOM; AP and JMK performed SP2 measurements of black carbon; TPB conducted meteorological measurements; RHM provided aerosol extinction measurements; AJS, EBW, EMG are the Fuel2Fire team and provided GOES-FRP diurnal patterns; DG and CAM provided TROPOMI CO emissions estimates; XY and PES provided forecast model estimates; TJS, MF, and JWH conducted HSRL measurements; RHS and SAM updated 3BEM_A19 to include updated emission factors; RA, EPJ, and GP provided HRRR-Smoke emissions; CES performed data analysis and wrote the manuscript.

Funding Sources and Acknowledgements. This work was supported in part by the NOAA Cooperative Agreement with CIRES, NA17OAR4320101. The University of Innsbruck team

was supported by the Austrian Federal Ministry for Transport, Innovation and Technology (bmvit, FFG, ASAP). F.P. received funding from the European Union's Horizon 2020 research and innovation program under grant agreement no. 674911 (IMPACT EU ITN). Tomas Mikoviny and Laura Tomsche provided field support. HG, PCJ and JLJ were supported by NASA grant 80NSSC18K0630. We thank Louisa Emmons and Christine Wiedinmyer for providing FINN v2.3 emissions and Shobha Kondragunta and Xiaoyang Zhang for GBBEPx emissions.

References

1. Andreae, M. O.; Merlet, P., Emission of trace gases and aerosols from biomass burning. *Global Biogeochem Cy* **2001,** *15*, (4), 955-966.
2. Bowman, D. M. J. S.; Balch, J. K.; Artaxo, P.; Bond, W. J.; Carlson, J. M.; Cochrane, M. A.; D'Antonio, C. M.; DeFries, R. S.; Doyle, J. C.; Harrison, S. P.; Johnston, F. H.; Keeley, J. E.; Krawchuk, M. A.; Kull, C. A.; Marston, J. B.; Moritz, M. A.; Prentice, I. C.; Roos, C. I.; Scott, A. C.; Swetnam, T. W.; van der Werf, G. R.; Pyne, S. J., Fire in the Earth System. *Science* **2009,** *324*, (5926), 481-484.
3. Abatzoglou, J. T.; Williams, A. P., Impact of anthropogenic climate change on wildfire across western US forests. *Proceedings of the National Academy of Sciences* **2016,** *113*, (42), 11770-11775.
4. Dennison, P. E.; Brewer, S. C.; Arnold, J. D.; Moritz, M. A., Large wildfire trends in the western United States, 1984-2011. *Geophysical Research Letters* **2014,** *41*, (8), 2928-2933.
5. Marlon, J. R.; Bartlein, P. J.; Gavin, D. G.; Long, C. J.; Anderson, R. S.; Briles, C. E.; Brown, K. J.; Colombaroli, D.; Hallett, D. J.; Power, M. J.; Scharf, E. A.; Walsh, M. K., Long-term perspective on wildfires in the western USA. *Proceedings of the National Academy of Sciences* **2012**.
6. Westerling, A. L.; Hidalgo, H. G.; Cayan, D. R.; Swetnam, T. W., Warming and earlier spring increase western US forest wildfire activity. *Science* **2006,** *313*, (5789), 940-943.
7. Aguilera, R.; Corringham, T.; Gershunov, A.; Benmarhnia, T., Wildfire smoke impacts respiratory health more than fine particles from other sources: observational evidence from Southern California. *Nature Communications* **2021,** *12*, (1), 1493.
8. Jaffe, D. A.; O'Neill, S. M.; Larkin, N. K.; Holder, A. L.; Peterson, D. L.; Halofsky, J. E.; Rappold, A. G., Wildfire and prescribed burning impacts on air quality in the United States. *Journal of the Air & Waste Management Association* **2020,** *70*, (6), 583-615.
9. Reid, C. E.; Considine, E. M.; Watson, G. L.; Telesca, D.; Pfister, G. G.; Jerrett, M., Associations between respiratory health and ozone and fine particulate matter during a wildfire event. *Environ Int* **2019,** *129*, 291-298.
10. Forster, P.; Ramaswamy, V.; Artaxo, P.; Berntsen, T.; Betts, R.; Fahey, D. W.; Haywood, J.; Lean, J.; Lowe, D. C.; Myhre, G.; Nganga, J.; Prinn, R.; Raga, G.; Schulz, M.; Van Dorland, R. *Changes in Atmospheric Constituents and in Radiative Forcing*; Cambridge University Press, Cambridge, United Kingdom and New York, NY, US: 2007.
11. Akagi, S. K.; Yokelson, R. J.; Wiedinmyer, C.; Alvarado, M. J.; Reid, J. S.; Karl, T.; Crounse, J. D.; Wennberg, P. O., Emission factors for open and domestic biomass burning for use in atmospheric models. *Atmos. Chem. Phys.* **2011,** *11*, (9), 4039-4072.

12. Bond, T. C., A technology-based global inventory of black and organic carbon emissions from combustion. *Journal of Geophysical Research* **2004,** *109*, (D14).
13. Bond, T. C.; Doherty, S. J.; Fahey, D. W.; Forster, P. M.; Berntsen, T.; DeAngelo, B. J.; Flanner, M. G.; Ghan, S.; Kärcher, B.; Koch, D.; Kinne, S.; Kondo, Y.; Quinn, P. K.; Sarofim, M. C.; Schultz, M. G.; Schulz, M.; Venkataraman, C.; Zhang, H.; Zhang, S.; Bellouin, N.; Guttikunda, S. K.; Hopke, P. K.; Jacobson, M. Z.; Kaiser, J. W.; Klimont, Z.; Lohmann, U.; Schwarz, J. P.; Shindell, D.; Storelvmo, T.; Warren, S. G.; Zender, C. S., Bounding the role of black carbon in the climate system: A scientific assessment. *Journal of Geophysical Research: Atmospheres* **2013,** *118*, (11), 5380-5552.
14. Balch, J. K.; Nagy, R. C.; Archibald, S.; Bowman, D. M.; Moritz, M. A.; Roos, C. I.; Scott, A. C.; Williamson, G. J., Global combustion: the connection between fossil fuel and biomass burning emissions (1997-2010). *Philos Trans R Soc Lond B Biol Sci* **2016,** *371*, (1696).
15. Page, S. E.; Siegert, F.; Rieley, J. O.; Boehm, H.-D. V.; Jaya, A.; Limin, S., The amount of carbon released from peat and forest fires in Indonesia during 1997. *Nature* **2002,** *420*, (6911), 61-65.
16. French, N. H. F.; de Groot, W. J.; Jenkins, L. K.; Rogers, B. M.; Alvarado, E.; Amiro, B.; de Jong, B.; Goetz, S.; Hoy, E.; Hyer, E.; Keane, R.; Law, B. E.; McKenzie, D.; McNulty, S. G.; Ottmar, R.; Pérez-Salicrup, D. R.; Randerson, J.; Robertson, K. M.; Turetsky, M., Model comparisons for estimating carbon emissions from North American wildland fire. *Journal of Geophysical Research* **2011,** *116*.
17. van der Werf, G. R.; Randerson, J. T.; Giglio, L.; Collatz, G. J.; Mu, M.; Kasibhatla, P. S.; Morton, D. C.; DeFries, R. S.; Jin, Y.; van Leeuwen, T. T., Global fire emissions and the contribution of deforestation, savanna, forest, agricultural, and peat fires (1997–2009). *Atmospheric Chemistry and Physics* **2010,** *10*, (23), 11707-11735.
18. Seiler, W.; Crutzen, P. J., Estimates of gross and net fluxes of carbon between the biosphere and the atmosphere from biomass burning. *Climatic Change* **1980,** *2*, (3), 207-247.
19. van Leeuwen, T. T.; van der Werf, G. R.; Hoffmann, A. A.; Detmers, R. G.; Rücker, G.; French, N. H. F.; Archibald, S.; Carvalho Jr, J. A.; Cook, G. D.; de Groot, W. J.; Hély, C.; Kasischke, E. S.; Kloster, S.; McCarty, J. L.; Pettinari, M. L.; Savadogo, P.; Alvarado, E. C.; Boschetti, L.; Manuri, S.; Meyer, C. P.; Siegert, F.; Trollope, L. A.; Trollope, W. S. W., Biomass burning fuel consumption rates: a field measurement database. *Biogeosciences* **2014,** *11*, (24), 7305-7329.
20. Hély, C.; Caylor, K.; Alleaume, S.; Swap, R. J.; Shugart, H. H., Release of gaseous and particulate carbonaceous compounds from biomass burning during the SAFARI 2000 dry season field campaign. *Journal of Geophysical Research: Atmospheres* **2003,** *108*, (D13).
21. Liu, T.; Mickley, L. J.; Marlier, M. E.; DeFries, R. S.; Khan, M. F.; Latif, M. T.; Karambelas, A., Diagnosing spatial biases and uncertainties in global fire emissions inventories: Indonesia as regional case study. *Remote Sensing of Environment* **2020,** *237*.
22. Pan, X.; Ichoku, C.; Chin, M.; Bian, H.; Darmenov, A.; Colarco, P.; Ellison, L.; Kucsera, T.; da Silva, A.; Wang, J.; Oda, T.; Cui, G., Six global biomass burning emission datasets: intercomparison and application in one global aerosol model. *Atmos. Chem. Phys.* **2020,** *20*, (2), 969-994.
23. van der Werf, G. R.; Randerson, J. T.; Giglio, L.; Collatz, G. J.; Kasibhatla, P. S.; Arellano Jr, A. F., Interannual variability in global biomass burning emissions from 1997 to 2004. *Atmos. Chem. Phys.* **2006,** *6*, (11), 3423-3441.
24. van der Werf, G. R.; Randerson, J. T.; Giglio, L.; van Leeuwen, T. T.; Chen, Y.; Rogers, B. M.; Mu, M.; van Marle, M. J. E.; Morton, D. C.; Collatz, G. J.; Yokelson, R. J.; Kasibhatla, P. S., Global fire emissions estimates during 1997–2016. *Earth System Science Data* **2017,** *9*, (2), 697-720.
25. Mota, B.; Wooster, M. J., A new top-down approach for directly estimating biomass burning emissions and fuel consumption rates and totals from geostationary satellite fire radiative power (FRP). *Remote Sensing of Environment* **2018,** *206*, 45-62.

26. Wooster, M. J.; Roberts, G.; Perry, G. L. W.; Kaufman, Y. J., Retrieval of biomass combustion rates and totals from fire radiative power observations: FRP derivation and calibration relationships between biomass consumption and fire radiative energy release. *Journal of Geophysical Research* **2005,** *110*, (D24).
27. Wooster, M., Fire radiative energy for quantitative study of biomass burning: derivation from the BIRD experimental satellite and comparison to MODIS fire products. *Remote Sensing of Environment* **2003,** *86*, (1), 83-107.
28. Freeborn, P. H.; Wooster, M. J.; Hao, W. M.; Ryan, C. A.; Nordgren, B. L.; Baker, S. P.; Ichoku, C., Relationships between energy release, fuel mass loss, and trace gas and aerosol emissions during laboratory biomass fires. *Journal of Geophysical Research* **2008,** *113*, (D1).
29. Ellicott, E.; Vermote, E.; Giglio, L.; Roberts, G., Estimating biomass consumed from fire using MODIS FRE. *Geophysical Research Letters* **2009,** *36*, (13).
30. Kaufman, Y. J.; Justice, C. O.; Flynn, L. P.; Kendall, J. D.; Prins, E. M.; Giglio, L.; Ward, D. E.; Menzel, W. P.; Setzer, A. W., Potential global fire monitoring from EOS-MODIS. *Journal of Geophysical Research: Atmospheres* **1998,** *103*, (D24), 32215-32238.
31. Roberts, G. J.; Wooster, M. J., Fire Detection and Fire Characterization Over Africa Using Meteosat SEVIRI. *IEEE Transactions on Geoscience and Remote Sensing* **2008,** *46*, (4), 1200-1218.
32. Schroeder, W.; Ellicott, E.; Ichoku, C.; Ellison, L.; Dickinson, M. B.; Ottmar, R. D.; Clements, C.; Hall, D.; Ambrosia, V.; Kremens, R., Integrated active fire retrievals and biomass burning emissions using complementary near-coincident ground, airborne and spaceborne sensor data. *Remote Sensing of Environment* **2014,** *140*, 719-730.
33. Ichoku, C., Quantitative evaluation and intercomparison of morning and afternoon Moderate Resolution Imaging Spectroradiometer (MODIS) aerosol measurements from Terra and Aqua. *Journal of Geophysical Research* **2005,** *110*, (D10).
34. Hudak, A. T.; Dickinson, M. B.; Bright, B. C.; Kremens, R. L.; Loudermilk, E. L.; O'Brien, J. J.; Hornsby, B. S.; Ottmar, R. D., Measurements relating fire radiative energy density and surface fuel consumption – RxCADRE 2011 and 2012. *International Journal of Wildland Fire* **2016,** *25*, (1).
35. Kaiser, J. W.; Heil, A.; Andreae, M. O.; Benedetti, A.; Chubarova, N.; Jones, L.; Morcrette, J. J.; Razinger, M.; Schultz, M. G.; Suttie, M.; van der Werf, G. R., Biomass burning emissions estimated with a global fire assimilation system based on observed fire radiative power. *Biogeosciences* **2012,** *9*, (1), 527-554.
36. Konovalov, I. B.; Berezin, E. V.; Ciais, P.; Broquet, G.; Beekmann, M.; Hadji-Lazaro, J.; Clerbaux, C.; Andreae, M. O.; Kaiser, J. W.; Schulze, E. D., Constraining CO2 emissions from open biomass burning by satellite observations of co-emitted species: a method and its application to wildfires in Siberia. *Atmospheric Chemistry and Physics* **2014,** *14*, (19), 10383-10410.
37. Ichoku, C.; Ellison, L., Global top-down smoke-aerosol emissions estimation using satellite fire radiative power measurements. *Atmospheric Chemistry and Physics* **2014,** *14*, (13), 6643-6667.
38. Ichoku, C.; Kaufman, Y. J., A method to derive smoke emission rates from MODIS fire radiative energy measurements. *IEEE Transactions on Geoscience and Remote Sensing* **2005,** *43*, (11), 2636-2649.
39. Ichoku, C.; Martins, J. V.; Kaufman, Y. J.; Wooster, M. J.; Freeborn, P. H.; Hao, W. M.; Baker, S.; Ryan, C. A.; Nordgren, B. L., Laboratory investigation of fire radiative energy and smoke aerosol emissions. *Journal of Geophysical Research* **2008,** *113*, (D14).
40. Bela, M. M.; Kille, N.; McKeen, S. A.; Romero-Alvarez, J.; Ahmadov, R.; James, E.; Pereira, G.; Schmidt, C.; Pierce, R. B.; O'Neill, S. M.; Zhang, X.; Kondragunta, S.; Wiedinmyer, C.; Volkamer, R., Quantifying Carbon Monoxide Emissions on the Scale of Large Wildfire. *Geophysical Research Letters* **submitted, 2021**.
41. Carter, T. S.; Heald, C. L.; Jimenez, J. L.; Campuzano-Jost, P.; Kondo, Y.; Moteki, N.; Schwarz, J. P.; Wiedinmyer, C.; Darmenov, A. S.; da Silva, A. M.; Kaiser, J. W., How emissions uncertainty influences the

distribution and radiative impacts of smoke from fires in North America. *Atmospheric Chemistry and Physics* **2020,** *20*, (4), 2073-2097.
42. Li, F.; Zhang, X.; Kondragunta, S.; Lu, X., An evaluation of advanced baseline imager fire radiative power based wildfire emissions using carbon monoxide observed by the Tropospheric Monitoring Instrument across the conterminous United States. *Environmental Research Letters* **2020,** *15*, (9).
43. Li, F.; Zhang, X.; Roy, D. P.; Kondragunta, S., Estimation of biomass-burning emissions by fusing the fire radiative power retrievals from polar-orbiting and geostationary satellites across the conterminous United States. *Atmospheric Environment* **2019,** *211*, 274-287.
44. Zhang, F.; Wang, J.; Ichoku, C.; Hyer, E. J.; Yang, Z.; Ge, C.; Su, S.; Zhang, X.; Kondragunta, S.; Kaiser, J. W.; Wiedinmyer, C.; da Silva, A., Sensitivity of mesoscale modeling of smoke direct radiative effect to the emission inventory: a case study in northern sub-Saharan African region. *Environmental Research Letters* **2014,** *9*, (7), 075002.
45. Peischl, J.; Ryerson, T. B.; Aikin, K. C.; Gouw, J. A.; Gilman, J. B.; Holloway, J. S.; Lerner, B. M.; Nadkarni, R.; Neuman, J. A.; Nowak, J. B.; Trainer, M.; Warneke, C.; Parrish, D. D., Quantifying atmospheric methane emissions from the Haynesville, Fayetteville, and northeastern Marcellus shale gas production regions. *Journal of Geophysical Research: Atmospheres* **2015,** *120*, (5), 2119-2139.
46. Conley, S.; Faloona, I.; Mehrotra, S.; Suard, M.; Lenschow, D. H.; Sweeney, C.; Herndon, S.; Schwietzke, S.; Pétron, G.; Pifer, J.; Kort, E. A.; Schnell, R., Application of Gauss's theorem to quantify localized surface emissions from airborne measurements of wind and trace gases. *Atmos. Meas. Tech.* **2017,** *10*, (9), 3345-3358.
47. Yokelson, R. J.; Burling, I. R.; Gilman, J. B.; Warneke, C.; Stockwell, C. E.; de Gouw, J.; Akagi, S. K.; Urbanski, S. P.; Veres, P.; Roberts, J. M.; Kuster, W. C.; Reardon, J.; Griffith, D. W. T.; Johnson, T. J.; Hosseini, S.; Miller, J. W.; Cocker Iii, D. R.; Jung, H.; Weise, D. R., Coupling field and laboratory measurements to estimate the emission factors of identified and unidentified trace gases for prescribed fires. *Atmos. Chem. Phys.* **2013,** *13*, (1), 89-116.
48. Gkatzelis, G. I., Parameterization of US wildfire and prescribed fire emissions based on FIREX-AQ aircraft measurements. *Atmos. Chem. Phys.* **in preparation, 2021**.
49. Pagonis, D.; Campuzano-Jost, P.; Guo, H.; Day, D. A.; Schueneman, M.; Nault, B. A.; Brown, W.; Laskin, A.; Siemens, K. S. A.; Coggon, M. M.; DiGangi, J. P.; Diskin, G. S.; Fenn, M. A.; Gkatzelis, G.; Hair, J. W.; Halliday, H. S.; Katich, J. M.; Nowak, J. B.; Perring, A. E.; Saide, P. E.; Sekimoto, K.; Shingler, T. J.; Thapa, L.; Warneke, C.; Jimenez, J. L., Chemical Aging of Biomass Burning Organic Aerosol: Insight from Fast Near-Molecular Measurements. In 2020; Vol. 2020, pp A234-01.
50. Andreae, M. O., Emission of trace gases and aerosols from biomass burning – an updated assessment. *Atmos. Chem. Phys.* **2019,** *19*, (13), 8523-8546.
51. Wiedinmyer, C.; Akagi, S. K.; Yokelson, R. J.; Emmons, L. K.; Al-Saadi, J. A.; Orlando, J. J.; Soja, A. J., The Fire INventory from NCAR (FINN): a high resolution global model to estimate the emissions from open burning. *Geoscientific Model Development* **2011,** *4*, (3), 625-641.
52. Wiedinmyer, C.; Kimura, Y.; McDonald-Buller, E.; Seto, K.; Emmons, L.; Tang, W.; Buccholz, R.; Orlando, J. J., The Fire INventory from NCAR version 2 (FINNv2): updates to a high resolution global fire emissions model. *Journal of Advances in Modeling Earth Systems* **In preparation**.
53. Darmenov, A.; da Silva, A., The quick fire emissions dataset (QFED) – Documentation of versions 2.1, 2.2 and 2.4. NASA. In Office, N. G. M. a. A., Ed. 2015; Vol. 38, p 183.
54. Ahmadov, R.; Grell, G.; James, E.; Csiszar, I.; Tsidulko, M.; Pierce, B.; McKeen, S.; Benjamin, S.; Alexander, C.; Pereira, G.; Freitas, S.; Goldberg, M. In *Using VIIRS fire radiative power data to simulate biomass burning emissions, plume rise and smoke transport in a real-time air quality modeling system*, 2017 IEEE International Geoscience and Remote Sensing Symposium (IGARSS), 23-28 July 2017, 2017; 2017; pp 2806-2808.

55. Zhang, X.; Kondragunta, S.; Da Silva, A.; Lu, S.; Ding, H.; Li, F.; Zhu, Y., The Blended Global Biomass Burning Emissions Product from MODIS, VIIRS, and Geostaionary Satellites (GBBEPx) Version 3.1. In 2021.
56. Walters, S. P.; Schneider, N. J.; Guthrie, J. D., Geospatial Multi-Agency Coordination (GeoMAC) wildland fire perimeters, 2008. *U.S. Geological Survey Data Series* **2011**, (6), 612.
57. Adams, C.; McLinden, C. A.; Shephard, M. W.; Dickson, N.; Dammers, E.; Chen, J.; Makar, P.; Cady-Pereira, K. E.; Tam, N.; Kharol, S. K.; Lamsal, L. N.; Krotkov, N. A., Satellite-derived emissions of carbon monoxide, ammonia, and nitrogen dioxide from the 2016 Horse River wildfire in the Fort McMurray area. *Atmos. Chem. Phys.* **2019,** *19*, (4), 2577-2599.
58. Griffin, D.; McLinden, C. A.; Dammers, E.; Adams, C.; Stockwell, C.; Warneke, C.; Bourgeois, I.; Peischl, J.; Ryerson, T. B.; Zarzana, K. J.; Rowe, J. P.; Volkamer, R.; Knote, C.; Kille, N.; Koenig, T. K.; Lee, C. F.; Rollins, D.; Rickly, P. S.; Chen, J.; Fehr, L.; Bourassa, A.; Degenstein, D.; Hayden, K.; Mihele, C.; Wren, S. N.; Liggio, J.; Akingunola, A.; Makar, P., Biomass burning nitrogen dioxide emissions derived from space with TROPOMI: methodology and validation. *Atmos. Meas. Tech. Discuss.* **2021,** *2021*, 1-44.
59. Kille, N.; Zarzana, K.; Romero Alvarez, J.; Lee, C.; Rowe, J.; Howard, B.; Campos, T.; Hills, A.; Hornbrook, R. S.; Ortega, I.; Permar, W.; Ku, I. T.; Lindaas, J.; Pollack, I.; Sullivan, A. P.; Zhou, Y.; Fredrickson, C.; Palm, B. B.; Peng, Q.; Apel, E.; Hu, L.; Collett, J.; Fischer, E.; Flocke, F.; Hannigan, J.; Thornton, J.; Volkamer, R., The CU Airborne Solar Occultation Flux Instrument: Performance evaluation during BB-FLUX. *ACS Earth and Space Chemistry* **2021**.
60. Wang, S.; Coggon, M. M.; Gkatzelis, G. I.; Warneke, C.; Bourgeois, I.; Ryerson, T.; Peischl, J.; Veres, P. R.; Neuman, J. A.; Hair, J.; Shingler, T.; Fenn, M.; Diskin, G.; Huey, L. G.; Lee, Y. R.; Apel, E. C.; Hornbrook, R. S.; Hills, A. J.; Hall, S. R.; Ullmann, K.; Bela, M. M.; Trainer, M. K.; Kumar, R.; Orlando, J. J.; Flocke, F. M.; Emmons, L. K., Chemical Tomography in a Fresh Wildland Fire Plume: A Large Eddy Simulation (LES) Study. *Journal of Geophysical Research: Atmospheres* **2021,** *126*, (18), e2021JD035203.
61. Borsdorff, T.; Aan de Brugh, J.; Hu, H.; Aben, I.; Hasekamp, O.; Landgraf, J., Measuring Carbon Monoxide With TROPOMI: First Results and a Comparison With ECMWF-IFS Analysis Data. *Geophysical Research Letters* **2018,** *45*, (6), 2826-2832.
62. Borsdorff, T.; aan de Brugh, J.; Hu, H.; Hasekamp, O.; Sussmann, R.; Rettinger, M.; Hase, F.; Gross, J.; Schneider, M.; Garcia, O.; Stremme, W.; Grutter, M.; Feist, D. G.; Arnold, S. G.; De Mazière, M.; Kumar Sha, M.; Pollard, D. F.; Kiel, M.; Roehl, C.; Wennberg, P. O.; Toon, G. C.; Landgraf, J., Mapping carbon monoxide pollution from space down to city scales with daily global coverage. *Atmospheric Measurement Techniques* **2018,** *11*, (10), 5507-5518.
63. Sha, M. K.; Langerock, B.; Blavier, J. F. L.; Blumenstock, T.; Borsdorff, T.; Buschmann, M.; Dehn, A.; De Mazière, M.; Deutscher, N. M.; Feist, D. G.; García, O. E.; Griffith, D. W. T.; Grutter, M.; Hannigan, J. W.; Hase, F.; Heikkinen, P.; Hermans, C.; Iraci, L. T.; Jeseck, P.; Jones, N.; Kivi, R.; Kumps, N.; Landgraf, J.; Lorente, A.; Mahieu, E.; Makarova, M. V.; Mellqvist, J.; Metzger, J. M.; Morino, I.; Nagahama, T.; Notholt, J.; Ohyama, H.; Ortega, I.; Palm, M.; Petri, C.; Pollard, D. F.; Rettinger, M.; Robinson, J.; Roche, S.; Roehl, C. M.; Röhling, A. N.; Rousogenous, C.; Schneider, M.; Shiomi, K.; Smale, D.; Stremme, W.; Strong, K.; Sussmann, R.; Té, Y.; Uchino, O.; Velazco, V. A.; Vrekoussis, M.; Wang, P.; Warneke, T.; Wizenberg, T.; Wunch, D.; Yamanouchi, S.; Yang, Y.; Zhou, M., Validation of Methane and Carbon Monoxide from Sentinel-5 Precursor using TCCON and NDACC-IRWG stations. *Atmos. Meas. Tech. Discuss.* **2021,** *2021*, 1-84.
64. Borsdorff, T.; aan de Brugh, J.; Schneider, A.; Lorente, A.; Birk, M.; Wagner, G.; Kivi, R.; Hase, F.; Feist, D. G.; Sussmann, R.; Rettinger, M.; Wunch, D.; Warneke, T.; Landgraf, J., Improving the TROPOMI CO data product: update of the spectroscopic database and destriping of single orbits. *Atmos. Meas. Tech.* **2019,** *12*, (10), 5443-5455.
65. Martínez-Alonso, S.; Deeter, M.; Worden, H.; Borsdorff, T.; Aben, I.; Commane, R.; Daube, B.; Francis, G.; George, M.; Landgraf, J.; Mao, D.; McKain, K.; Wofsy, S., 1.5 years of TROPOMI CO measurements: comparisons to MOPITT and ATom. *Atmos. Meas. Tech.* **2020,** *13*, (9), 4841-4864.

66. Jin, X.; Zhu, Q.; Cohen, R., Direct estimates of biomass burning NOx emissions and lifetime using daily observations from TROPOMI. *Atmos. Chem. Phys. Discuss.* **2021,** *2021*, 1-27.
67. Theys, N.; Volkamer, R.; Müller, J. F.; Zarzana, K. J.; Kille, N.; Clarisse, L.; De Smedt, I.; Lerot, C.; Finkenzeller, H.; Hendrick, F.; Koenig, T. K.; Lee, C. F.; Knote, C.; Yu, H.; Van Roozendael, M., Global nitrous acid emissions and levels of regional oxidants enhanced by wildfires. *Nature Geoscience* **2020,** *13*, (10), 681-686.
68. Wiggins, E. B.; Soja, A. J.; Gargulinski, E.; Halliday, H. S.; Pierce, R. B.; Schmidt, C. C.; Nowak, J. B.; DiGangi, J. P.; Diskin, G. S.; Katich, J. M.; Perring, A. E.; Schwarz, J. P.; Anderson, B. E.; Chen, G.; Crosbie, E. C.; Jordan, C.; Robinson, C. E.; Sanchez, K. J.; Shingler, T. J.; Shook, M.; Thornhill, K. L.; Winstead, E. L.; Ziemba, L. D.; Moore, R. H., High Temporal Resolution Satellite Observations of Fire Radiative Power Reveal Link Between Fire Behavior and Aerosol and Gas Emissions. *Geophysical Research Letters* **2020,** *47*, (23), e2020GL090707.
69. Ye, X.; Arab, P.; Ahmadov, R.; James, E.; Grell, G. A.; Pierce, B.; Kumar, A.; Makar, P.; Chen, J.; Davignon, D.; Carmichael, G.; Ferrada, G.; McQueen, J.; Huang, J.; Kumar, R.; Emmons, L.; Herron-Thorpe, F. L.; Parrington, M.; Engelen, R.; Peuch, V. H.; da Silva, A.; Soja, A.; Gargulinski, E.; Wiggins, E.; Hair, J. W.; Fenn, M.; Shingler, T.; Kondragunta, S.; Lyapustin, A.; Wang, Y.; Holben, B.; Giles, D.; Saide, P. E., Evaluation and intercomparison of wildfire smoke forecasts from multiple modeling systems for the 2019 Williams Flats fire. *Atmos. Chem. Phys. Discuss.* **2021,** *2021*, 1-69.
70. Saide, P. E.; Peterson, D. A.; da Silva, A.; Anderson, B.; Ziemba, L. D.; Diskin, G.; Sachse, G.; Hair, J.; Butler, C.; Fenn, M.; Jimenez, J. L.; Campuzano-Jost, P.; Perring, A. E.; Schwarz, J. P.; Markovic, M. Z.; Russell, P.; Redemann, J.; Shinozuka, Y.; Streets, D. G.; Yan, F.; Dibb, J.; Yokelson, R.; Toon, O. B.; Hyer, E.; Carmichael, G. R., Revealing important nocturnal and day-to-day variations in fire smoke emissions through a multiplatform inversion. *Geophysical Research Letters* **2015,** *42*, (9), 3609-3618.
71. Randerson, J. T.; Chen, Y.; van der Werf, G. R.; Rogers, B. M.; Morton, D. C., Global burned area and biomass burning emissions from small fires. *Journal of Geophysical Research: Biogeosciences* **2012,** *117*, (G4).
72. Reddington, C. L.; Spracklen, D. V.; Artaxo, P.; Ridley, D. A.; Rizzo, L. V.; Arana, A., Analysis of particulate emissions from tropical biomass burning using a global aerosol model and long-term surface observations. *Atmospheric Chemistry and Physics* **2016,** *16*, (17), 11083-11106.
73. Jordan, N. S.; Ichoku, C.; Hoff, R. M., Estimating smoke emissions over the US Southern Great Plains using MODIS fire radiative power and aerosol observations. *Atmospheric Environment* **2008,** *42*, (9), 2007-2022.
74. Vermote, E.; Ellicott, E.; Dubovik, O.; Lapyonok, T.; Chin, M.; Giglio, L.; Roberts, G. J., An approach to estimate global biomass burning emissions of organic and black carbon from MODIS fire radiative power. *Journal of Geophysical Research* **2009,** *114*, (D18).
75. Lu, X.; Zhang, X.; Li, F.; Cochrane, M. A., Investigating Smoke Aerosol Emission Coefficients Using MODIS Active Fire and Aerosol Products: A Case Study in the CONUS and Indonesia. *Journal of Geophysical Research: Biogeosciences* **2019,** *124*, (6), 1413-1429.
76. Permar, W.; Wang, Q.; Selimovic, V.; Wielgasz, C.; Yokelson, R. J.; Hornbrook, R. S.; Hills, A. J.; Apel, E. C.; Ku, I.-T.; Zhou, Y.; Sive, B. C.; Sullivan, A. P.; Collett Jr, J. L.; Campos, T. L.; Palm, B. B.; Peng, Q.; Thornton, J. A.; Garofalo, L. A.; Farmer, D. K.; Kreidenweis, S. M.; Levin, E. J. T.; DeMott, P. J.; Flocke, F.; Fischer, E. V.; Hu, L., Emissions of Trace Organic Gases From Western U.S. Wildfires Based on WE-CAN Aircraft Measurements. *Journal of Geophysical Research: Atmospheres* **2021,** *126*, (11), e2020JD033838.
77. Kremens, R. L.; Dickinson, M. B.; Bova, A. S., Radiant flux density, energy density and fuel consumption in mixed-oak forest surface fires. *International Journal of Wildland Fire* **2012,** *21*, (6).
78. Li, F.; Zhang, X.; Kondragunta, S.; Roy, D. P., Investigation of the Fire Radiative Energy Biomass Combustion Coefficient: A Comparison of Polar and Geostationary Satellite Retrievals Over the Conterminous United States. *Journal of Geophysical Research: Biogeosciences* **2018,** *123*, (2), 722-739.

79. Zhang, X.; Kondragunta, S.; Ram, J.; Schmidt, C.; Huang, H.-C., Near-real-time global biomass burning emissions product from geostationary satellite constellation. *Journal of Geophysical Research: Atmospheres* **2012,** *117*, (D14).
80. Xu, L., Ozone Chemistry in Western U.S. wildfire plumes. *Science Advances* **submitted, 2021**.
81. Lindaas, J.; Pollack, I. B.; Garofalo, L. A.; Pothier, M. A.; Farmer, D. K.; Kreidenweis, S. M.; Campos, T. L.; Flocke, F.; Weinheimer, A. J.; Montzka, D. D.; Tyndall, G. S.; Palm, B. B.; Peng, Q.; Thornton, J. A.; Permar, W.; Wielgasz, C.; Hu, L.; Ottmar, R. D.; Restaino, J. C.; Hudak, A. T.; Ku, I.-T.; Zhou, Y.; Sive, B. C.; Sullivan, A.; Collett Jr, J. L.; Fischer, E. V., Emissions of Reactive Nitrogen From Western U.S. Wildfires During Summer 2018. *Journal of Geophysical Research: Atmospheres* **2021,** *126*, (2), e2020JD032657.